Laboratory study of wave-induced drift of large floating objects

Qian Xiao[1], Mark McAllister[1], Thomas Adcock[1], and Ton van den Bremer[1,2] [1]

Department of Engineering Science, University of Oxford, Oxford, OX1 3PJ, UK

[2] Department of Civil Engineering and Geosciences, TU Delft,
Stevinweg 1, 2628 CN Delft, The Netherlands

E-mail Address: qian.xiao@eng.ox.ac.uk

1. INTRODUCTION

Every year millions tonnes of plastic waste enter the oceans. The plastic paradox arises from the mismatch between the observed amount of plastics in the world's oceans and the emissions of plastic from land into the ocean [1]. Unraveling the global plastic mass transfer budget and oceanic plastic budget necessitates a better understanding of the physical processes governing mass transport including wave-induced transport [2]. A floating object in the ocean, exposed to waves, undergoes drift in addition to its oscillatory motion. The drift of these objects can be expected to be affected by their various sizes and shapes, leading to non-Lagrangian drift behaviour [3, 4, 5]. In this study, we present the laboratory measurements of wave-induced drift for large two-dimensional floating objects. We study deep-water, unidirectional, regular waves with wave steepness ($\epsilon = ka_w$, where k is the wavenumber and a_w is the wave amplitude) ranging from 0.04 to 0.31 to investigate the effects of size and wave steepness on drift behaviour. To do this, we used a group of objects with a rectangular cross-section and a constant aspect ratio but varying in characteristic length from 2.6% to 27.1% of the incident wavelength are used. A different drift behaviour for small and large objects is observed, with a regime shift at a certain size and wave steepness. The experimental results are interpreted by comparison with the standard theoretical Stokes drift and a theoretical model of "diffraction modified Stokes drift" [6]. We discuss the mechanisms involved in enhanced drift based on these interpretations.

2. STUDY APPROACHES (METHODOLOGY)

2.1 Experimental setup The experimental tests were conducted in the 10 m long, 1.1 m wide and 0.85 m deep Wave and Current Flume at the University of Oxford, UK. Two E2-4K Ultra HD Cinematic Cameras (Z-CAM-E1503) were utilized to measure the movement of the floating objects with one positioned on the side and one on the top. Computer vision techniques, including image processing, object detection, object tracking and edge detection, were applied to obtain the experiment data and object drifts. To maintain the two-dimensional (2D) nature of our experiments, we designed the width of our floating objects to match that of the flume. Bearings were installed at each end (left and right end) of the objects to minimize friction and collisions between the objects and the side walls of the flume. This design also aimed to prevent objects from rotating around the vertical direction. As a means to measure the strength of Eulerian currents at the surface, small three-dimensional (3D) floating balls (diameter $l = 0.02$ m) with a size of 1% of the wavelength were utilized as current drogues.

A total of 48 wave conditions were examined across four different frequencies: 0.9 Hz, 1.00 Hz, 1.05 Hz and 1.10 Hz. For each frequency, 12 different wave steepness values ranging from 0.04 to 0.32 were used, with a 0.02 interval for ka_w values between 0.04 and 0.2 and an interval of 0.04 for ka_w values between 0.2 to 0.31. By varying the size of the object l and the incident wavelength λ, we obtain a range of relative object sizes l/λ. The experimental matrix, detailing different object size and wave conditions is provided in table 1.

2.2 Theoretical models For an idealized fluid parcel, the leading order of standard Stokes drift in finite water depth for regular waves is given by $u_S = c(a_w k)^2 \frac{\cosh(2k(d+z))}{2\sinh^2(kd)}$, where $c = \omega/k$ is the wave celerity, $\omega = 2\pi f$ the angular frequency, z the vertical coordinate of the fluid particle. In deep

l/λ [%]	1.05	2.62	3.21	3.55	3.88	5.24	8.43	10.52	12.48	15.58	18.32	22.44	24.82	27.13
f (Hz)	0.9	0.9	1.0	1.05	1.1	0.9	0.9	0.9	1.1	1.1	0.9	1.0	1.05	1.1
l (m)	0.02	0.050	0.05	0.05	0.05	0.100	0.161	0.201	0.161	0.201	0.350	0.350	0.350	0.350
λ (m)	1.91	1.91	1.56	1.41	1.29	1.91	1.91	1.91	1.29	1.29	1.91	1.56	1.41	1.29

Table 1: Matrix of relative object size l/λ. For each relative object size, experiments covers 12 different wave steepness were performed. For a frequency of f=0.90 Hz, wave amplitudes range from $0.012 - 0.094$ m, resulting in ka_w values spanning 0.04 to 0.31; Similarly, for $f = 1.0$ Hz, wave amplitudes range from $0.010 - 0.079$ m with ka_w values between 0.04 and 0.32; The frequency $f = 1.05$ Hz, wave amplitudes ranging from $0.009 - 0.072$ m, ka_w=0.04$-$0.32 and frequency $f = 1.10$ Hz, wave amplitude ranging from $0.007 - 0.064$ m, ka_w=0.03$-$0.31.
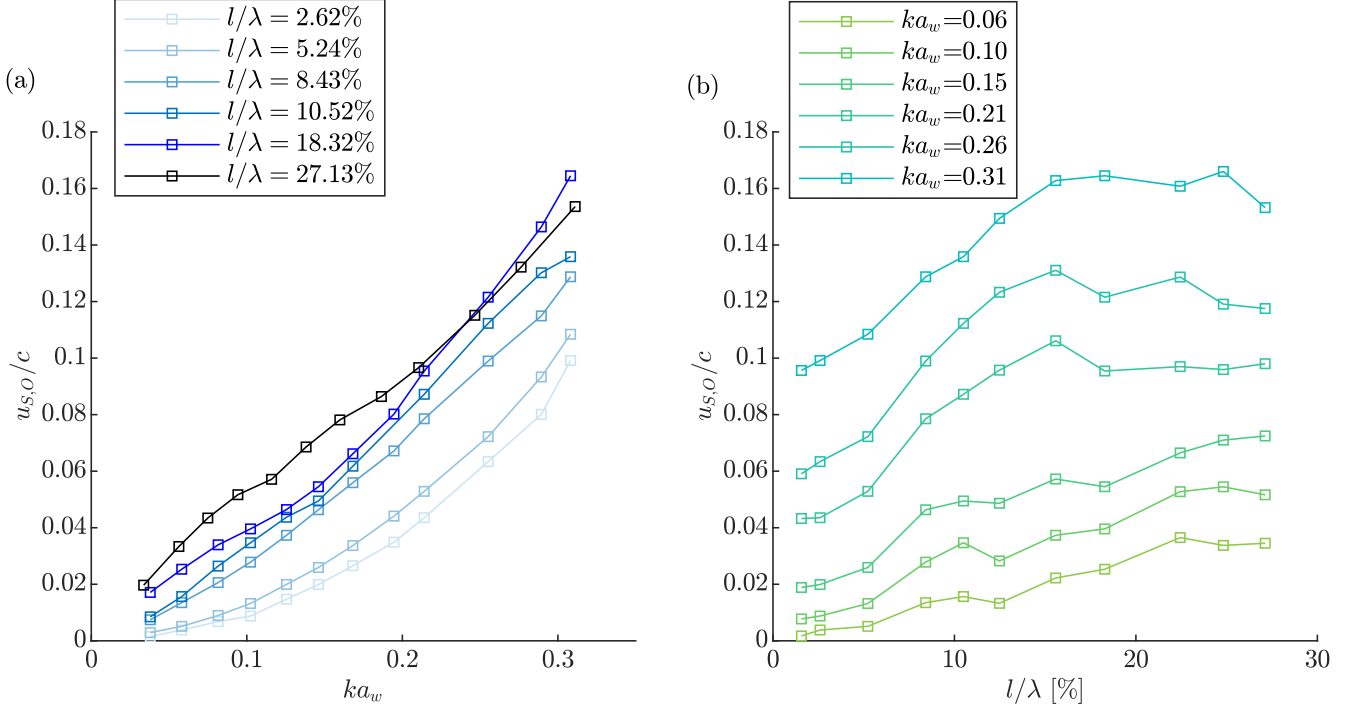

Figure 1: Celerity-normalized Stokes object drift velocity (a) as a function of wave steepness for different object relative size (b) as a function of relative size for different wave steepness.

water ($kd \gg 1$), it simplifies to $u_S = c(a_w k)^2 e^{2kz}$. A theoretical model known as diffraction-modified Stokes drift (DMS) has been derived by [6]. This model predicts an object drift as a 'Stokes object drift' akin to the standard Stokes drift, but accounting for the combination of incident, diffracted and radiated wave fields. The modified Stokes object drift is calculated by:

$$u_{S,O,DMS} = \overline{\xi_x \frac{\partial^2 \Phi}{\partial x^2} + \xi_z \frac{\partial^2 \Phi}{\partial x \partial z}} = \overline{\xi_x \left(\frac{\partial^2 \Phi_I}{\partial x^2} + \frac{\partial^2 \Phi_R}{\partial x^2} + \frac{\partial^2 \Phi_D}{\partial x^2} \right) + \xi_z \left(\frac{\partial^2 \Phi_I}{\partial x \partial z} + \frac{\partial^2 \Phi_R}{\partial x \partial z} + \frac{\partial^2 \Phi_D}{\partial x \partial z} \right)}, \quad (1)$$

where ξ_x and ξ_z are the linear horizontal and vertical harmonic oscillatory motions of the object, respectively; And Φ_I, Φ_R, Φ_D represent the incident, radiation and diffraction potential, respectively. In the current study, we use a linear boundary element method to solve the diffracted and radiated fields. Thus non-linear effects are not captured in this model.

3. RESULTS AND ANALYSIS
The experimental measurements presented here focus on the drift velocity of the objects. These measurements are compared with the predictions of the two theoretical models mentioned above to
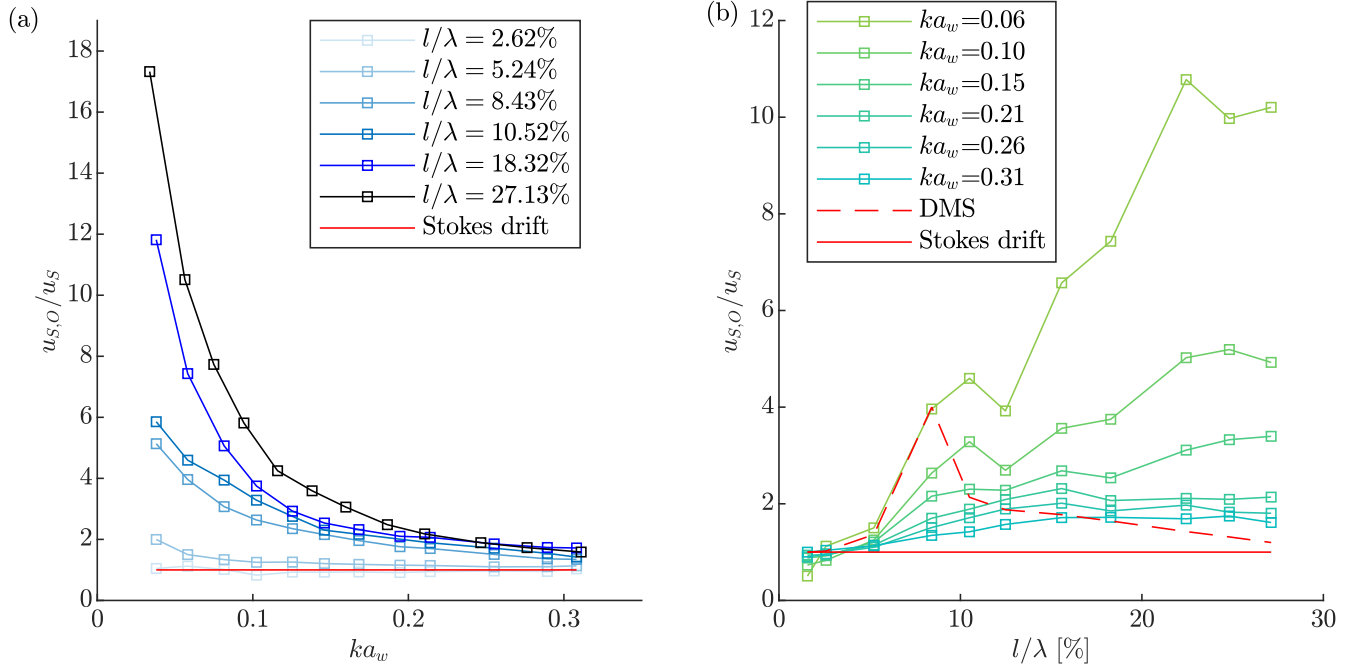
Figure 2: Stokes drift-normalized Stokes object drift velocity (a) as a function of wave steepness for different object relative size (b) as a function of relative size for different wave steepness. The theoretical Stokes drift value u_S remains constant for all cases in both (a) and (b), represented by red lines. The red dashed line labeled 'DMS' signifies results from diffraction-modified Stokes drift $u_{O,S,DMS}$ by equation (1). Notably, 'DMS' results remain consistent for a specific object size across different wave steepness values (we use linear 'BEM' model to solve equation (1)), resulting in a single line in (b).

interpret the results and explore the effects of object size and wave steepness. Note that not all measured data are reported here and plotted on the figures to improve clarity and readability.

The mean Lagrangian drift of the object, denoted as $\overline{u}_{L,O}$ is derived from its horizontal trajectory extracted from the videos recorded by cameras. After reaching a quasi-steady state, a low-frequency filter is applied to the original trajectory data, and a linear regression is performed on the subharmonic signal to obtain the time-averaged drift $\overline{u}_{L,O}$. The Stokes object drift $u_{S,O}$ is then evaluated as $u_{S,O} = \overline{u}_{L,O} - \overline{u}_E$ (cf. [7]), where $\overline{u}_E$ is the Eulerian-mean velocity on the flume surface. The Eulerian-mean velocity $\overline{u}_E$ in different wave conditions employed here is examined using small balls as current drogues, previously shown to behave as accurate Lagrangian tracers (cf. [8]).

Effects of size and wave steepness: We begin by examining the Stokes object drift normalized by wave celerity, plotted as a function of object size and wave steepness in figure 1. The drift shows a clear dependence on both object size and wave steepness. There are critical values for both wave steepness and size, at which the drift behaves differently before and after. According to figure 1 (a), the drift monotonically increases with wave steepness but the rate of increase varies for different object sizes. For small objects (e.g. $l/\lambda = 2.62\%$), the increasing pattern appears quadratic, whereas for larger objects (e.g. $l/\lambda{=}27.13$ %), it is closer to linear. This is qualitatively consistent with the experimental results reported by [9]. Based on figure 1 (b), in low wave steepness (e.g. $ka_w < 0.15$), the Stokes object drift increases with relative size up to 27.13%. However, in relatively high wave steepness, the drift initially increases with relative size for $l/\lambda \leq 15.58\%$ but exhibits a decreasing/constant trend for even larger objects.

Comparison with theoretical models: Figure 2 compares the laboratory experimental results to two theoretical models: standard Stokes drift u_S and diffraction-modified Stokes drift $u_{S,O,DMS}$.

In figure 2 (a), it is observed that, for very small objects, the drift closely adheres to the standard Stokes drift, maintaining a constant value of 1 across varying wave steepness. However, as the object size increases, particularly for smaller wave steepness (e.g. $ka_w \leq 0.15$), the amplification factor $u_{S,O}/u_S$ rises, indicating significant drift enhancement. For objects with a size $l/\lambda \geq 5.24\%$, within the low to intermediate wave steepness range ($e.g. 0.03 \leq ka_w \leq 0.15$), an increase in wave steepness leads to a drastic reduction in the amplification factor $u_{S,O}/u_S$. Beyond this range, with further increases in wave steepness, the amplification factor either stabilizes or decreases gradually, resulting in a distinctive peak value at the lowest wave steepness. This decreasing pattern is most pronounced for the largest objects ($l/\lambda = 27.13\%$), aligning with findings in the experimental results by [4].
Moreover, figure 2 reveals that for a certain wave steepness, the amplification factor increases with size but the increasing pattern varies for different wave steepness. For higher steepness, a steady increase is observed, while for lower wave steepness, the amplification exhibits a rapid ascent. The theoretical prediction of diffraction-based modified Stokes drift aligns reasonably with experimental results for small objects sizes $l/\lambda \leq 8.43\%$ but only under specific wave steepness conditions. However, notable disparities emerge for larger objects, especially at higher wave steepness, revealing a more complex set of behaviors not captured by the theoretical model predictions.

4. CONCLUSIONS

1. The object's drift is a function of both object relative size and wave steepness. When the object is small ($l/\lambda = 2.62\%$), it consistently follows Stokes drift across all measured wave steepness values. For larger objects ($l/\lambda \leq 8.42\%$), the observed enhanced drift aligns reasonably well with diffraction-modified Stokes drift [6] although this explanation falls short in accurately predicting drift enhancement for larger objects.
2. Contrary to the quadratic dependence predicted by standard Stokes drift, the dependence of drift behavior on wave steepness is found to be a combination of linear and quadratic, with variations based on relative size.
3. The amplification of drift relative to standard Stokes drift $u_{S,O}/u_S$ reaches its peak at the lowest wave steepness and subsequently decreases with increasing wave steepness, stabilizing at a constant value or exhibiting a slow decreasing rate.

REFERENCES

[1] Jambeck, J. R., Geyer, R., Wilcox, C., Siegler, T. R., Perryman, M., Andrady, A., Narayan, R., and Law, K. L. 2015. *Plastic waste inputs from land into the ocean.* Science 347(6223), 768–771.
[2] Kaandorp, M. L., Lobelle, D., Kehl, C., Dijkstra, H. A., and van Sebille, E. 2023. *Global mass of buoyant marine plastics dominated by large long-lived debris.* Nature Geoscience 16(8), 689–694.
[3] Stokes, G. G. 1847. *On the theory of oscillatory waves. Trans. Camb. Phil. Soc. 8*, 411–455.
[4] Huang, G., Law, A. W., and Huang, Z. 2011. *Wave-induced drift of small floating objects in regular waves.* Ocean Eng. 38(4), 712–718.
[5] Calvert, R., McAllister, M. L., Whittaker, C., Raby, A., Borthwick, A. G. L., and van den Bremer, T. S. 2021. *A mechanism for the increased wave-induced drift of floating marine litter. J. Fluid Mech. 915*.
[6] Xiao, Q., Calvert, R., Yan, S. Q., Adcock, T. A. A., and van den Bremer, T. S. 2024. *Surface gravity wave-induced drift of floating objects in the diffraction regime. J.Fluid Mech. 980*, A27.
[7] Bühler, O. 2014. *Waves and Mean Flows*, 2nd ed. Cambridge University Press, Cambridge, UK.
[8] Alsina, J., Jongedijk, C. E., and van Sebille, E. 2020. *Laboratory Measurements of the Wave-Induced Motion of Plastic Particles: Influence of Wave Period, Plastic Size and Plastic Density.* J. Geophys. Res-Oceans 125(12), e2020JC016294.
[9] He, M., Ren, B., and Qiu, D. 2016. *Experimental study of nonlinear behaviors of a free-floating body in waves.* China Ocean Eng. 30(3), 421–430.